Chemical Engineering Journal 395 (2020) 125078

Contents lists available at ScienceDirect

Chemical Engineering Journal

journal homepage: www.elsevier.com/locate/cej

Photocatalytic degradation of gaseous VOCs over Tm^{3+}-TiO_2: Revealing the activity enhancement mechanism and different reaction paths

Zepeng Rao[a,b], Gansheng Shi[a], Zhuang Wang[a], Asad Mahmood[a], Xiaofeng Xie[a,*], Jing Sun[a,*]

[a] State Key Lab of High Performance Ceramics and Superfine Microstructure, Shanghai Institute of Ceramics, Chinese Academy of Sciences, 1295 Dingxi Road, Shanghai 200050, China

[b] University of Chinese Academy of Sciences, 19 (A) Yuquan Road, Beijing 100049, China

HIGHLIGHTS

- The decreased particle size of Tm-TiO_2 enhanced the adsorption capability towards VOCs.
- Improved charge separation was ascribed to the induced 4f-states of Tm ions.
- More hydrophilicity of Tm-TiO_2 produced more •OH radicals.
- The photodegradation pathway of VOCs on Tm-modified TiO_2 was proposed.

GRAPHICAL ABSTRACT

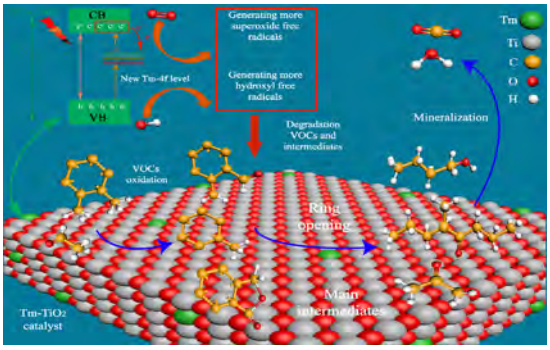

ARTICLE INFO

Keywords:
Tm-TiO_2 catalyst
Acetaldehyde
O-xylene
Mixed VOCs
Reaction paths

ABSTRACT

In this work, we synthesized thulium (Tm^{3+}) modified TiO_2 nanoparticles by a facile sol-gel route. We show that Tm^{3+}-modified TiO_2 exhibit superior photocatalytic activity than pure TiO_2 towards gas-phase degradation of acetaldehyde, *o*-xylene, and their mixture. The photocatalytic activity enhances with the increasing Tm content from 0.1 to 0.5 mol%. The 0.5 mol%Tm-TiO_2 sample demonstrated the highest photodegradation efficiency (> 90.0%) for acetaldehyde and *o*-xylene. According to the systematic characterization such as photoluminescence (PL), photocurrent, up-conversion spectra, UV–Vis diffuse reflectance spectroscopy and electron spin resonance (ESR) analysis, the enhanced photocatalytic performance can be attributed to introducing the new Tm-4f states between the original band gap of TiO_2, which led to the increase of efficiency of light-induced electron-hole separation and the increase of hydrophilicity which resulted in the increased adsorption capacity towards acetaldehyde and *o*-xylene. Gas Chromatography-Mass Spectrometer (GC–MS) analysis suggested that *o*-xylene was first oxidized to *o*-benzaldehyde, which was eventually converted to butanol before being mineralized into CO_2. However, new intermediates including phthalide, *o*-methyl acetophenone, naphthalene and 5-Methyl-4-octanone were detected in the mixture.

1. Introduction

Volatile organic compounds (VOCs) are produced in the environment through various sources, including fossil fuel processing, industrial and agricultural operations, and automobile exhaust gases [1]. The presence of VOCs in the outdoors and indoor environment can

* Corresponding authors.
E-mail addresses: xxfshcn@163.com (X. Xie), jingsun@mail.sic.ac.cn (J. Sun).

https://doi.org/10.1016/j.cej.2020.125078
Received 26 December 2019; Received in revised form 23 March 2020; Accepted 12 April 2020
Available online 15 April 2020
1385-8947/

cause serious health issues, such as cancer, respiratory, liver and skin problems. It is reported that VOCs are accountable for the ozone depletion and also contribute to secondary aerosol formation [2–4]. Therefore, it is important to eliminate VOCs from the outdoors as well as the indoor environment. To do this, several technologies have been developed, for example, adsorption, thermal catalysis and photocatalysis [3]. Among these, photocatalytic oxidation (PCO) is regarded as a promising method for the destruction of VOCs [5–7], which utilize oxide semiconductor materials, i.e., TiO_2, Cu_2O, Fe_2O_3, WO_3 and ZnO to harvest solar light at ambient temperature [4]. The hole-electron pairs (h^+/e^-) produced in these materials can either directly oxidize the pollutant molecules or produce reactive oxygen species, i.e., hydroxyl (•OH) and superoxide ($•O_2^-$) radicals [4]. These reactive radicals further participate in the surface catalyzed reaction.

TiO_2 has been regarded as a potential photocatalyst for the solution as well as gas-phase photocatalytic reactions to degrade environmental pollutants due to its high oxidation capacity, non-toxicity, low cost, and chemical stability [8–10]. However, the practical use of TiO_2 is still hindered by low light-harvesting capability, which can only harvest light in the UV region ($\lambda < 380$ nm) of the solar spectrum. The fast recombination of photogenerated hole-electron pairs further limits its usefulness. The incorporation of rare earth (RE) ions in the crystal lattice of TiO_2 is an effective way to tailor the optical bandgap of TiO_2 and hence to improve the light-harvesting and charge separation properties [11–13]. Along these lines, different RE ions, i.e., Nd^{3+}, Pr^{3+}, Ho^{3+}, Er^{3+} and Tm^{3+}, have been used as dopants in TiO_2 crystal lattice to improve the photocatalytic performance of TiO_2 [14–24]. The studies suggested that the superior photocatalytic performance of RE ions-doped TiO_2 is attributed to the up-conversion process (UCP), in which low energy photons are converted to high energy photons One such attempt was reported by the Obregon et al. [17]. They studied the photodegradation of liquid-phase phenol and gas-phase toluene using Er-doped TiO_2. Their results suggested an improved photocatalytic activity of Er-doped TiO_2 in contrast to pure TiO_2, which was attributed to the up-conversion phenomenon. In other studies, TiO_2 doped with various Tm content were synthesized by ball-mill [19] and low-temperature hydrolysis methods [20,21]. It has been observed that Tm-doped TiO_2 exhibited 50% high photodegradation efficiency in contrast to pure TiO_2 to photodegrade methylene blue under an actinic lamp irradiation [20]. On the other hand, the improved photocatalytic activity of RE ions doped TiO_2 nanoparticles is related to the incorporation of impurity states (RE-4f level) around the Fermi level in the optical bandgap of TiO_2. These impurity states either facilitates the conduction of photoinduced electrons or trap them, which eventually improve the charge separation efficiency. Parnicka et al. [14] investigated the UCP in Nd-TiO_2 samples during liquid-phase phenol photodegradation. They reported that although Nd-TiO_2 could be excited in the visible region (400 to 480 nm), the UCP was not responsible for the enhancement of photocatalytic performance. Mazierski et al. [15] reviewed that the UCP would not affect the photocatalytic properties because of the low intensity of the RE emission. Liu et al. [18] also reported an improved photodegradation of phenol in the aqueous phase under visible light irradiation utilizing Tm-doped TiO_2 nanoparticles. Despite these attempts, the PCO of gas-phase VOCs is widely ignored on Tm ions doped TiO_2 nanoparticles. Also, the role of Tm ions in the enhancement of photocatalytic activity continues to be dubious. Similarly, Tm doped TiO_2 has been rarely studied and most of the related studies investigated the photocatalytic performance of Tm-TiO_2 nanoparticle for the solution phase dyes degradation [18–21]. Therefore, it is meaningful to investigate the photocatalytic degradation pathways and interaction of organic pollutants with Tm ions doped TiO_2 nanoparticles to comprehend the photodegradation mechanism in depth.

Herein, we synthesized TiO_2 nanoparticles with varying Tm content (0.1–0.5 mol%). In this way, we significantly improved the photocatalytic activity of TiO_2 for the removal of gas-phase VOCs, which include acetaldehyde, *o*-xylene and their mixture. The as-prepared nanoparticles demonstrated superior adsorption capabilities, improved charge separation, and high photocatalytic activities with xenon lamp (400 W) irradiation in contrast to pure TiO_2. We found an enhanced hydrophilic character in Tm-modified TiO_2 nanoparticles, which particularly benefit for the adsorption capacity. The detected intermediates suggested that VOCs degraded through different paths on pure TiO_2 and Tm-modified TiO_2, which could be associated with the variation in chemical structure and hydrophilic affinity of catalysts. Our study explored in detail how Tm doping improved the photocatalytic performance of TiO_2. The proposed oxidation pathways further highlight the photocatalytic oxidation mechanism of the gas-phase VOCs.

2. Experimental

2.1. Materials

The precursor materials were used without further purification. We used titanium (IV) isopropoxide (TIP) (97%, Sigma–Aldrich) and Tm $(NO_3)_3{\cdot}6H_2O$ (99.9%, Sigma–Aldrich) as titanium and Tm sources. Acetic acid and ethanol (Zhenxing Co., Ltd) were used as solvents. 5,5-dimethyl-1-pyrroline N-oxide (DMPO) (Sigma Chemical Co.) was used as radicals trapping agent.

2.2. Preparation of Tm-TiO_2

Pure and Tm-doped TiO_2 were synthesized via a sol-gel method. In a typical procedure, TIP (10 mL) was first dissolved in a mixture of ethanol (46 mL) and acetic acid (6 mL) under magnetic stirring. Then distilled water (3 mL) was added to the above solution. Next, a certain amount of Tm $(NO_3)_3{\cdot}6H_2O$ was added and kept under vigorous stirring for 60 min. The as-prepared solution was aged for 90 min, which was subsequently converted to dried gel in an electric oven at 60 °C for 24 h. The dried gel was transferred into a muffle furnace and calcined at 500 °C for 2 h to achieve the final product. The samples with a different Tm mole ratio are noted as pure TiO_2 and 0.1%Tm-TiO_2, 0.3%Tm-TiO_2, and 0.5%Tm-TiO_2.

2.3. Characterization

The X-ray diffraction (XRD) profiles were collected on a diffractometer (Bruker, D8 Advance) using Cu Ka irradiation ($\lambda = 0.15418$ nm) in the range of 2θ from 20° to 80°. The Brunauer–Emmett–Teller (BET) specific surface area (S_{BET}) analysis of the photocatalysts was performed on a Micromeritics ASAP 3000 apparatus. Raman spectra were obtained using a DXR spectrometer under the excitation of laser wavelength $\lambda_{ex} = 532$ nm. A field-emission scanning electron microscope (FESEM, Magellan 400) was used to analyze the morphology of the samples. The microstructure of the photocatalysts was investigated by a high-resolution transmission electron microscope (HRTEM; JEM-2100) using 200 kV as an accelerating voltage. A Lambda 950 spectrometer (Perkin–Elmer) equipped with $BaSO_4$ as reference was used to characterize the UV–vis spectra. The up-conversion spectra were taken using a FLS 980 instrument. X-ray photoelectron spectroscopy (XPS) analysis was carried out by a Perkin Elmer system (PHI-5000C ESCA) with a monochromatic MgKα X-ray source, the binding energy was calibrated with C 1 s (BE = 284.6 eV) signals of contaminant carbon. PL spectra were measured by the luminescence spectrometer 55 (LS55, Perkin–Elmer) under an excitation wavelength of 250 nm. The photocurrent response curve and electrochemical impedance spectroscopy (EIS) were carried out in a slandered three-electrode cell using an electrochemical workstation (CHI660D) equipped with an AM1.5G solar power system. ESR spectra were recorded on a JES-FA200 spectrometer. Initially, sample (4 mg) was dispersed in a mixture containing DMPO (40 μL) and 4 mL of ethanol (for DMPO- $•O_2^-$) or deionized water (for DMPO- •OH) under

irradiation for 3 min. The temperature-programmed desorption (TPD) test was performed on a ChemiSorb PCA-1200 measurement to investigate the adsorption–desorption behavior of the samples. The intermediate species during the photodegradation reaction were studied using a GC–MS (TSQ 8000 Evo, Thermo).

2.4. Adsorption capacity and photocatalytic activity

The adsorption and photodegradation properties of acetaldehyde, *o*-xylene and mixed acetaldehyde and *o*-xylene were tested in a continuous automatic intake reactor (Scheme S1). The dynamic adsorption–desorption experiments were performed in the dark to investigate the adsorption behavior of our samples. In a typical procedure, we added 120 mg of sample into a 50 mL of plastic bottle containing 12 mL of ethanol, which was tightly sealed. The suspension was ball milled for 8 h. Finally, the as-prepared samples (0.1 g) were coated on a glass substrate and dried in an electric oven at 80 °C. The coated glass samples were transferred to the reaction chamber, which were tightly capped. The sample gases were allowed to flow (flow rate: 20 sccm) through the reaction chamber. Initially, the adsorption–desorption equilibrium was achieved in the dark. Next, the samples were irradiated using a UV–visible light (400 W xenon lamp) source. The distance between the lamp and the surface of the catalyst is 31 cm and the incident integrated irradiance of the lamp on the sample surface is 51.2 mW/cm^2. In this measurement, the initial concentration of all VOCs was 25 ppm. The adsorption capacity (A_c) of VOCs was calculated by the Eq. (1):

$$A_c = C_0 \times \rho_1 \times \rho_2 \times \left[\int_0^t \nu \times (1 - C/C_0)dt\right]_{catalyst} - \left[\int_0^t \nu \times (1 - C/C_0)dt\right]_{blank} /(M \times m) \quad (1)$$

The conversion efficiency (Ƞ) of target VOC is calculated by the Eq. (2),

$$\eta = (C_0 - C)/C_0 \times 100\% \quad (2)$$

The photodegradation rate follows a pseudo-first-order kinetic model as according to the Eq. (3):

$$ln(C_0/C) = rt. \quad (3)$$

where C_0 is the initial concentration of VOC, C represents the concentration at different time intervals, ρ_1 and ρ_2 are the air density and the relative vapor density of VOC, ν represent VOC flow rate, M and m are the VOC molar mass and photocatalyst mass, r and *t* are the reaction rate constant and time interval, respectively.

3. Results and discussion

3.1. Structural and morphology characteristics of photocatalysts

The XRD and HRTEM results confirmed pure anatase phase for all the samples (Figs. 1a and S1). The average crystallite size was calculated by the Scherrer equation and the results are given in Table 1. The average crystallite size decreased from 24.3 to 16.0 nm with increasing Tm content. As the ionic radius of Ti^{4+} (61 pm) is smaller than that of Tm^{3+} (87 pm), therefore, it is difficult to incorporate Tm^{3+} in the crystal lattice of TiO_2. It has been previously reported that the mismatch of ionic radii could result in Ti-O-Tm bonds (i.e., surface modification) or formation of Tm_2O_3 at the grain boundaries [25]. Accordingly, it is anticipated that the formation of Ti-O-Tm bonds or Tm_2O_3 might inhibit the growth of TiO_2 grains. This behavior might be responsible for the decreased crystallite size, which consequently increased the specific surface area from 26.301 to 56.895 m^2/g with increasing Tm content (Table 1). The Rietveld refinement method was used to evaluate the effect of Tm content on the unit cell parameters (Table 1). The unit cell volume increased slightly from 136.01 to 136.72 Å^3 with increasing Tm concentration, which suggested that Tm ions might induce interstitial doping. Similar results have been previously reported [26,27]. Therefore, it can be inferred that Tm doping in TiO_2 resulted in interstitial doping and surface modification under the given experimental conditions.

The Raman spectra further confirmed that all of the samples retained pure anatase phase during the calcination process, which exhibited characteristic Raman modes ($3E_g + 2B_{1g} + A_{1g}$) of anatase phase (Fig. 1b). The well-resolved distinct Raman bands at 144, 395, 516, and 638 cm^{-1} and a weaker peak at 197 cm^{-1} were assigned to $E_{g(1)}$, B_{1g}, A_{1g}/B_{1g}, $E_{g(3)}$ and $E_{g(2)}$ vibrational modes of TiO_2 , respectively, where E_g, A_{1g}, and B_{1g} modes were attributed to the symmetric stretching, symmetric and asymmetric bending vibrations of O–Ti–O, respectively [28–30].

The SEM micrographs and particle size distribution histograms are given in Fig. 2. In contrast to pure TiO_2 (26.5 nm), the mean particle size of Tm-doped samples decreased from 24.2 to 16.2 nm with increasing Tm content (Fig. 2a–d), which suggested that Tm doping inhibited the grain growth. These results are in good agreement with the XRD data.

Fig. 3 shows the absorption properties of pure and Tm-doped TO_2. We observed three additional bands in the range from 400 to 1100 nm in Tm doped samples, which could be attributed to f-f electronic transitions of Tm^{3+} ions. The adsorption peaks at 467, 685 and 796 nm could be associated with the transitions from the Tm ion ground state $^3H_6$ to the higher energy levels $^1G_4$, $^3F_{2/3}$ and $^3H_4$, respectively [31,32]. Hence, it can be inferred that Tm^{3+} ions were successfully incorporated in the host crystal lattice of TiO_2. Interestingly, the absorption edge of Tm-doped TiO_2 slightly shifted to low energy wavelengths compared with pure TiO_2 (Fig. 3b). This behavior contradicted the previous reports which have reported a red shift for somewhat similar compositions [33,34]. The blue shift might be associated with the surface modification by successive Tm doping and small crystallite size. Despite this effect, the doping of Tm ions in TiO_2 did not result in a significant change of the optical band [17,35]. Remarkably, no up-conversion phenomenon could be evidenced in 0.5%Tm-modified TiO_2 sample under laser λ_{ex} at 467, 685 and 796 nm excitation (Fig. S2), indicating that the enhanced photocatalytic performance of Tm-doped TiO_2 is not related to the UCP effect.

The XPS spectra are shown in Figs. 4 and S3. The bands at ~464.20 eV and ~458.50 eV were assigned to Ti $2p_{1/2}$ and Ti $2p_{3/2}$ of Ti^{4+}–O bonds (Fig. S3a) [36,37], respectively. The three peaks of C 1 s XPS spectra at 288.19, 286.46 and 284.60 eV were associated with C = O, C–OH and C–C, respectively (Fig. S3b) [38]. The presence of these peaks might be associated with the organic residues during the calcination process or the atmospheric gas adsorption. Although there exist carbonaceous species in all samples, the presence of carbonaceous species did not affect the physicochemical properties of the catalyst [39].

A broad band of O 1 s XPS spectra can be resolved into two peaks, which were attributed to surface Ti-OH groups (O_{OH}, at 531.36 eV) and surface lattice oxygen (O_L, at 529.63 eV), respectively (Fig. 4a). The ratio of O_{OH} / (O_{OH} + O_L) can be roughly used to interpret the hydrophilicity or polarity of materials [40,41]. As listed in Table 1, the ratio of O_{OH}/O_L increased from 0.09 to 0.34 with increasing Tm content, which suggested that the surface hydrophilicity of the catalysts increased. We further confirmed this behavior by contact angle (Fig. S4). The smaller the contact angle, the stronger the hydrophilicity. A significant decrease in the contact angle from 11.58° to 5.66° was observed in Tm-modified samples in comparison with pure TiO_2, illustrating that the hydrophilicity of the material was enhanced. This characteristic is useful for better interaction between the photocatalyst and polar molecules. A weak Tm_2O_3 peak can be found at approximately 177.11 eV only in 0.5%Tm-TiO_2 sample (Fig. 4b) [20,42], which

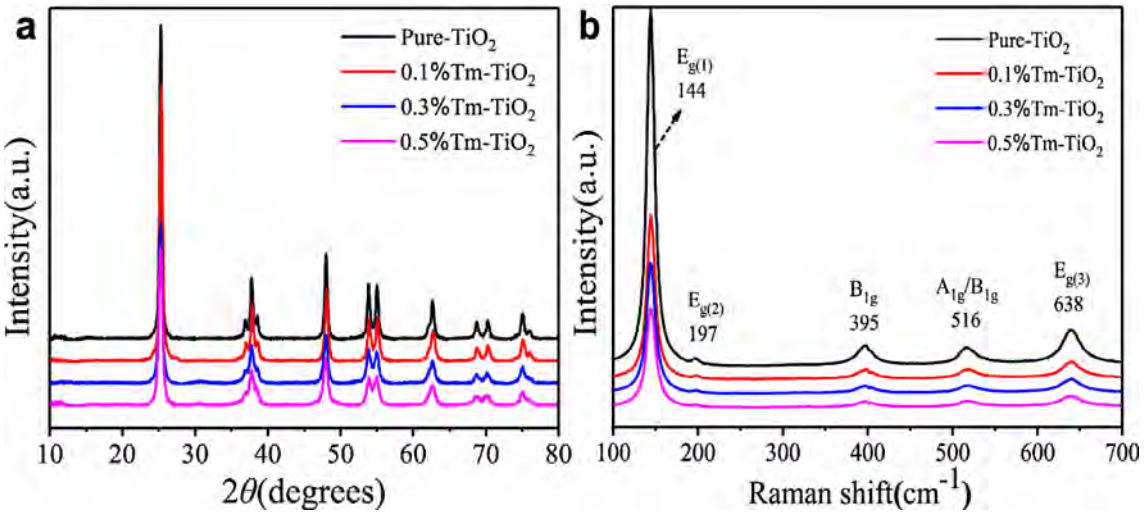

Fig. 1. (a) XRD and (b) Raman spectra of pure and Tm-modified TiO_2 samples.

Table 1
Structural cell parameters, the specific surface area (S_{BET}) and XPS results of pure and Tm-modified TiO_2 samples.

Sample	V (Å^3)	Crystallite size (nm)	S_{BET} (m^2/g)	O_{OH}: (O_{OH} + O_L)	Tm (Atomic %)
pure-TiO_2	136.01	24.3	26.301	0.09	0
0.1%Tm-TiO_2	136.52	23.2	35.286	0.14	0
0.3%Tm-TiO_2	136.70	19.1	46.643	0.21	0
0.5%Tm-TiO_2	136.72	16.0	58.895	0.34	0.04

suggested the formation of Tm_2O_3 on the surface of Tm-doped TiO_2 catalysts. However, Tm_2O_3 could not be detected in 0.1% and 0.3% Tm-modified samples due to its lower concentration.

3.2. PL and photoelectrochemical properties

The migration, capture and recombination of photoinduced carriers in photocatalytic materials are one of the major factors in photocatalytic processes, and these features were investigated by PL and photoelectrochemical measurements. Fig. 5a displays that the intensity of PL spectra for the as-prepared catalysts gradually decreased after the

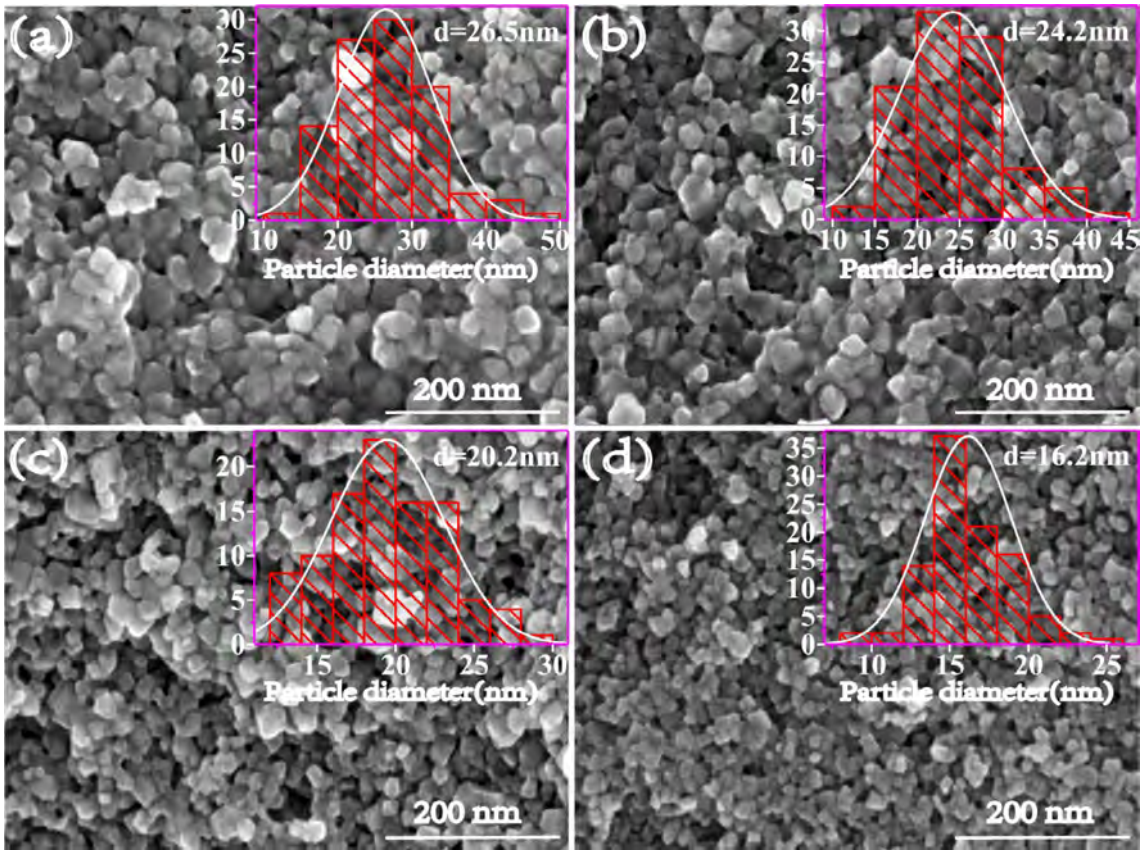

Fig. 2. SEM images of (a) pure-TiO_2, (b) 0.1%Tm-TiO_2, (c) 0.3%Tm-TiO_2, (d) 0.5%Tm-TiO_2. The inset figures show the particle size distribution of the samples.

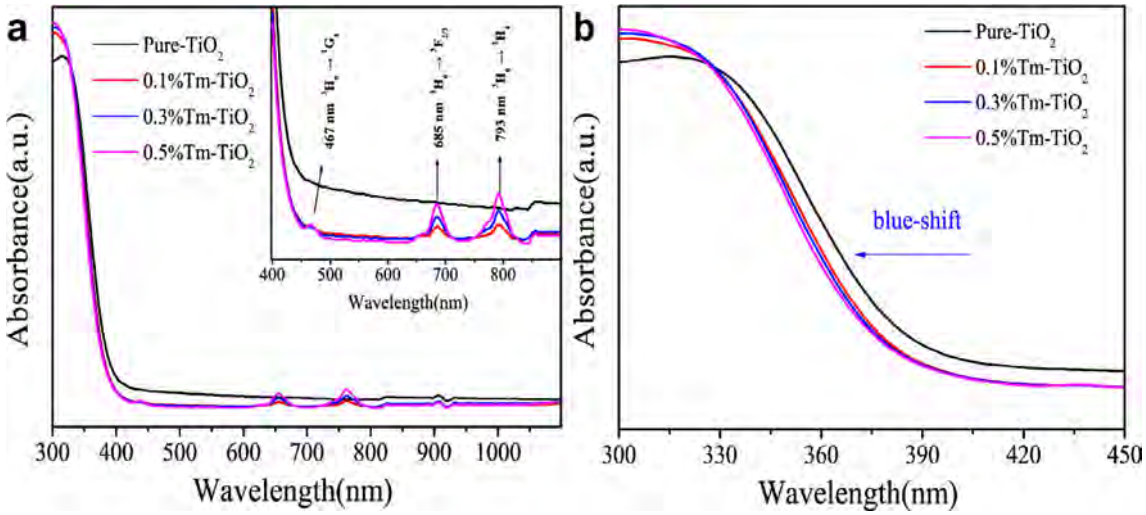

Fig. 3. (a) UV–vis spectra and (b) the spectra at 300–450 nm of all photocatalysts under 250 nm excitation.

addition of Tm ions, which suggested that the separation process of photoinduced electron-hole pairs was improved. This might be due to the incorporation of new Tm-4f levels or intra-4f electrons of Tm ions facilitating the photoinduced carries transfer-transition between TiO_2 and Tm ion [43–45]. The photocurrent density curves and EIS data further verified this mechanism. As shown in Fig. 5b, the photocurrent density of the samples increased with increasing Tm concentration, which also confirmed that the incorporation of Tm in TiO_2 crystal lattice promoted the photogenerated electron-hole pairs' separation [46,47]. The EIS results revealed that the photogenerated charge separation efficiency increased with the increase of Tm content (Fig. S5). Therefore, it can be inferred that Tm doping can promote the separation and migration of electron-hole pairs.

3.3. The adsorption capacity of single VOC

The adsorption of VOCs on a photocatalyst surface is critical for the gas-phase photocatalytic reaction. The difference in degradation results (including removal efficiency, degradation rate and path) is closely related to the chemical structure of a pollutant gas molecule and adsorption behavior on the photocatalyst surface. We used dynamic adsorption and TPD experiments to evaluate the adsorption properties of pure and Tm-doped TiO_2 samples. Fig. 6a and b show the dynamic adsorption plots of single acetaldehyde and *o*-xylene (25 ppm, 20 sccm), respectively. The adsorption capacity of pure TiO_2 improved when doped with Tm, which could be due to increasing specific surface area and the polarity of the catalyst surface (Table 1). Two selected VOCs exhibited the highest adsorption ability on 0.5% Tm-TiO_2 (3.635 μmol/g and 2.116 μmol/g for acetaldehyde and *o*-xylene, respectively) in contrast to pure TiO_2 (1.083 μmol/g and 0.770 μmol/g for acetaldehyde and *o*-xylene, respectively), which was 2.4 and 1.7 times higher for acetaldehyde and *o*-xylene, respectively. The adsorption amount of acetaldehyde was higher than that of *o*-xylene, which is related to the size (molecular weight) and polarity of acetaldehyde molecules [48]. The size of acetaldehyde molecule is smaller than *o*-xylene and the polarity of acetaldehyde molecule is greater than *o*-xylene. Moreover, since our samples exhibited surface polarity, which will strongly interact with acetaldehyde molecules in contrast to weakly polar *o*-xylene molecules.

The TPD experiment exhibited the different desorption peaks in the temperature range from 80 to 400 ℃ for acetaldehyde (Fig. 6c) and from 60 to 980 ℃ for *o*-xylene (Fig. 6d). The adsorption capacity of acetaldehyde and *o*-xylene increased with increasing Tm content, suggesting that Tm doping enhanced the adsorption capacity. The TCD signals of acetaldehyde were higher than *o*-xylene, which indicated that greater quantity acetaldehyde was adsorbed than *o*-xylene. The TPD results are in good agreement with the dynamic adsorption test. The desorption peaks for Tm-doped samples around 350 ℃ (acetaldehyde)

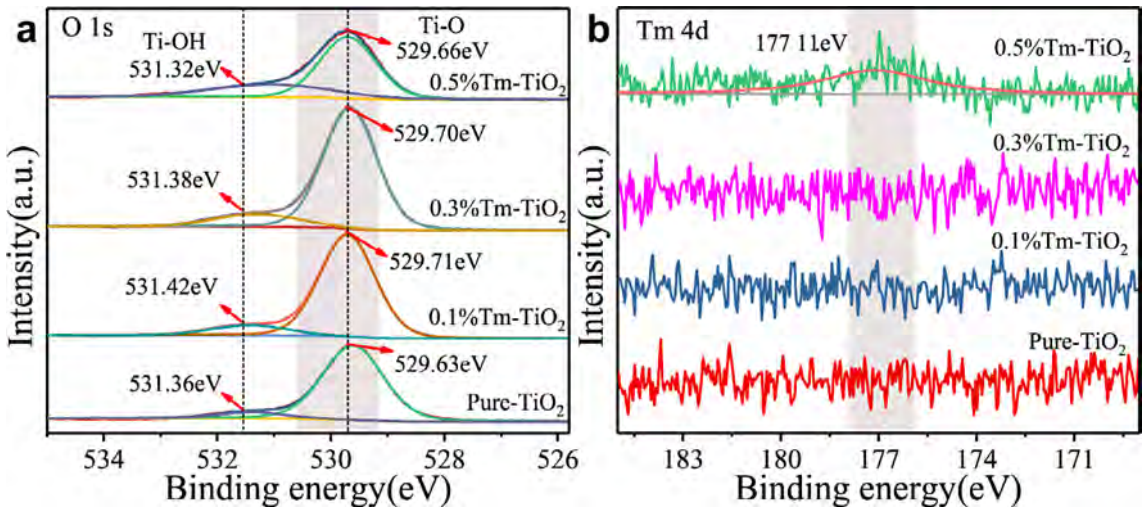

Fig. 4. (a) XPS data for (a) O 1 s and (b) Tm 4d regions of the as-prepared photocatalysts.

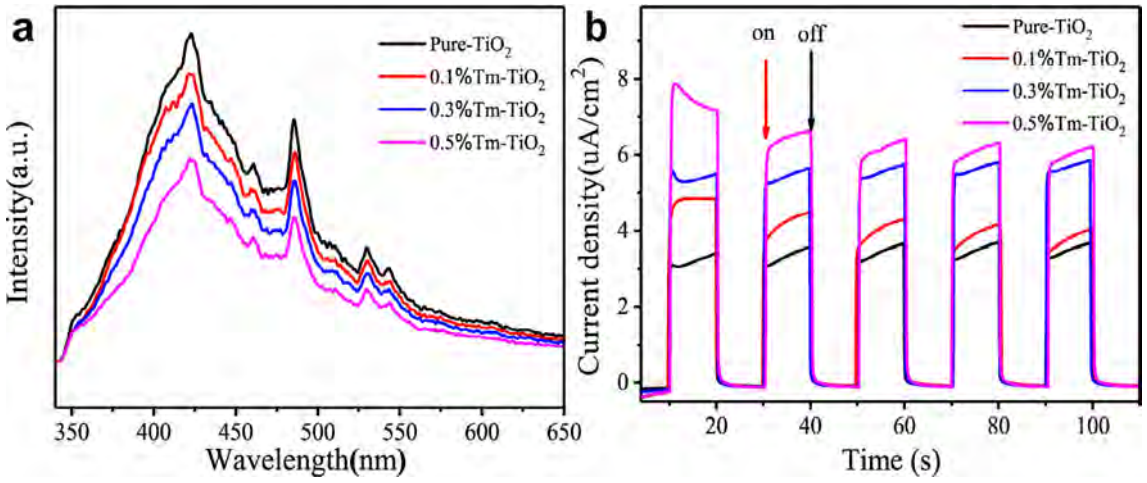

Fig. 5. (a) Photoluminescence emission spectra and (b) photocurrent density curves of pure and Tm-modified TiO_2 samples.

and 790 °C (*o*-xylene) were different from pure TiO_2 which appeared around 200 °C for acetaldehyde and 600 °C for *o*-xylene, indicating improved chemical adsorption capabilities of Tm modified TiO_2. Based on these results, it can be inferred that Tm doping significantly improved the adsorption properties of TiO_2, which will eventually affect the photodegradation efficiency.

3.4. Photocatalytic properties of single VOC

Fig. 7 shows that Tm doping enhanced the photocatalytic properties of TiO_2. The removal efficiency of pure TiO_2, 0.1%, 0.3% and 0.5%Tm-doped TiO_2 for acetaldehyde was 51.1%, 85.8%, 95.9% and 99.2%, respectively (Fig. 7a and Table 2). The order of degradation rate (min^{-1}) was as follows: TiO_2 (0.0167) < 0.1%Tm-TiO_2

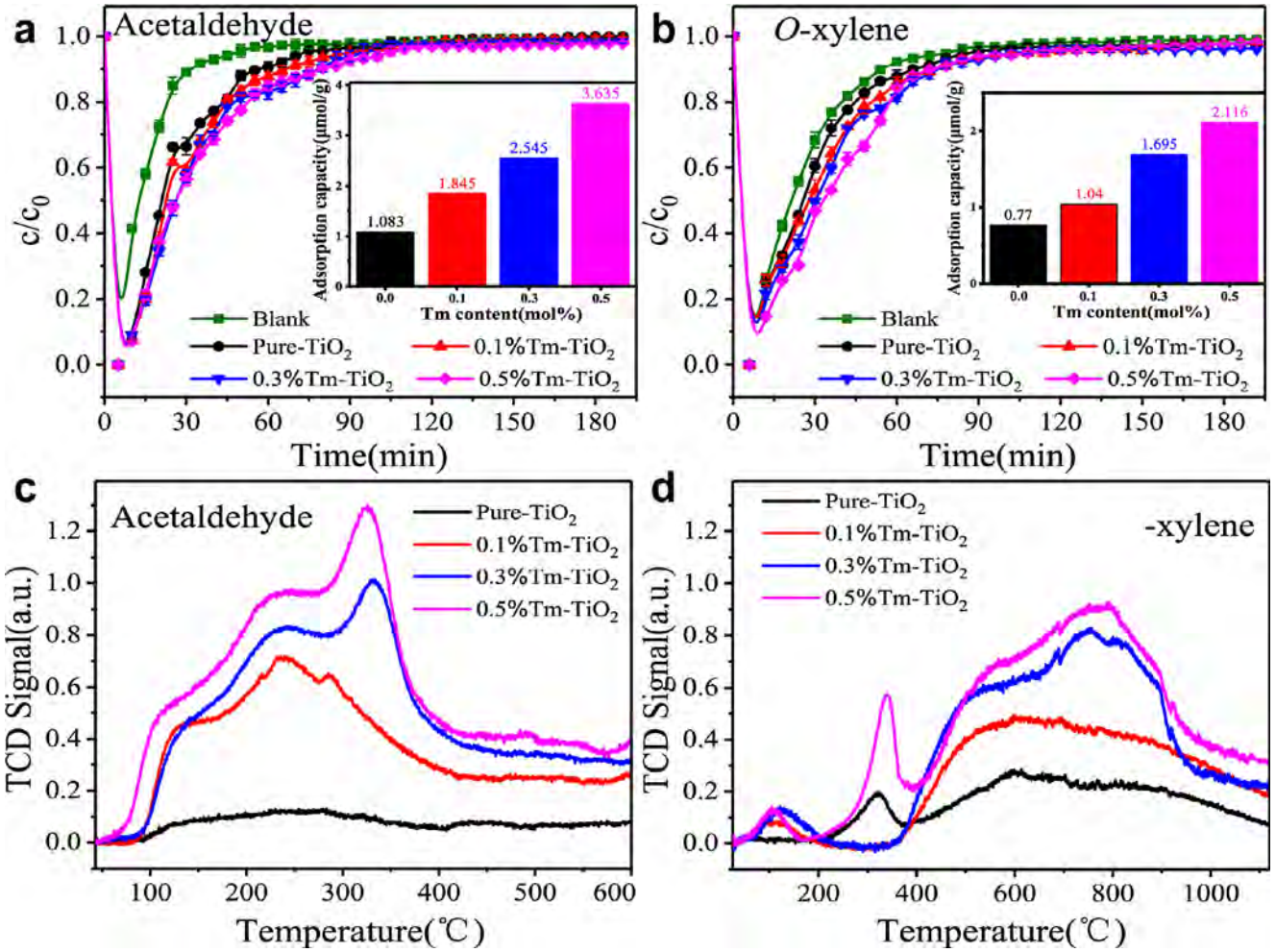

Fig. 6. Dynamic adsorption plots of (a) acetaldehyde and (b) *o*-xylene, the inset shows the corresponding adsorption amount of gas-phase VOC, and acetaldehyde -TPD (c) *o*-xylene -TPD (d) curves. The initial concentration of VOC is 25 ppm.

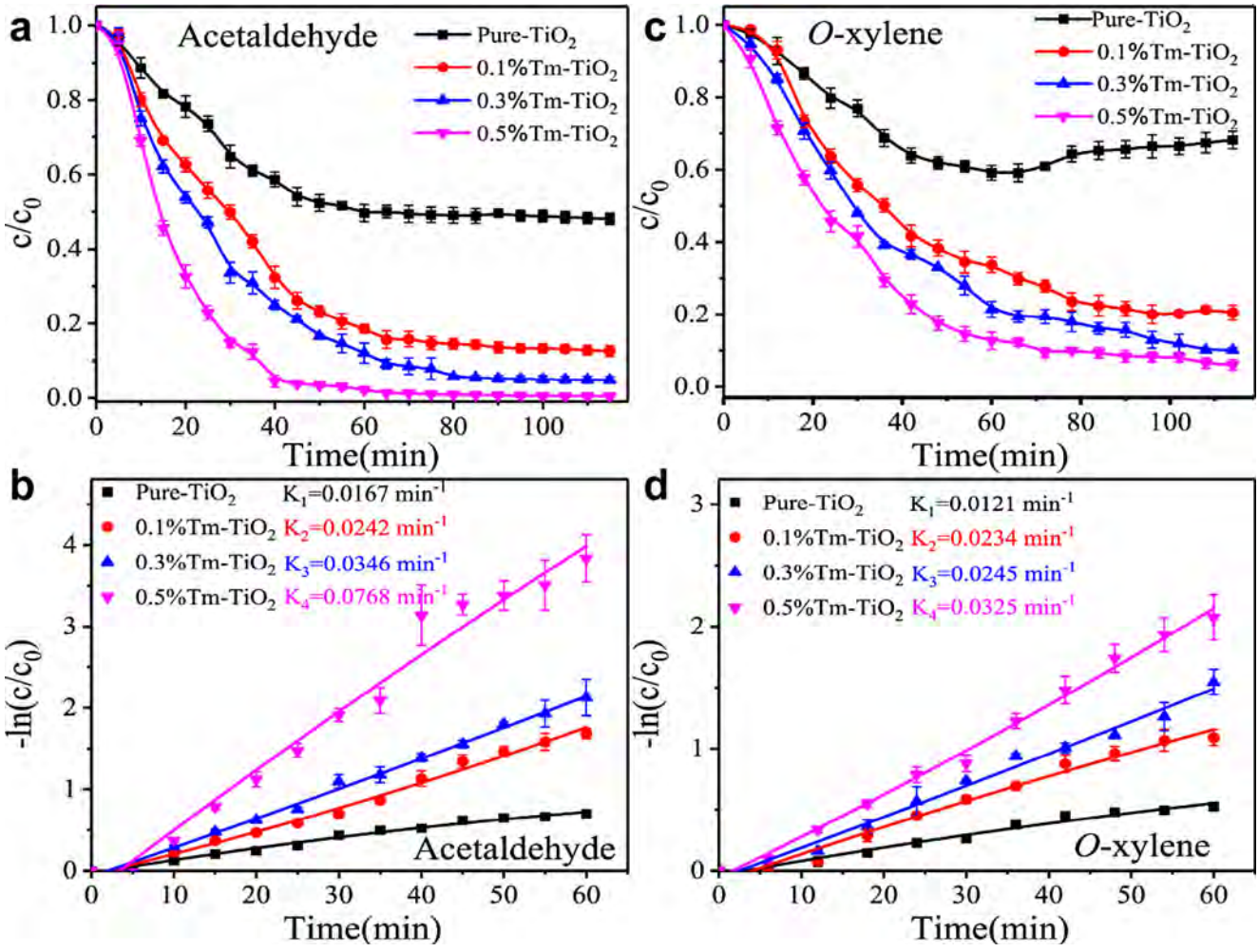

Fig. 7. The photodegradation plots for the flowing gas-phase (a) acetaldehyde and (b) *o*-xylene at a flowing rate of 20 sccm under the light illumination, quasi-first-order kinetic model of (c) acetaldehyde and (d) *o*-xylene within 60 min.

(0.0242) < 0.3%Tm-TiO_2 (0.0346) < 0.5%Tm-TiO_2 (0.0768), respectively (Fig. 7b). Similarly, the order of *o*-xylene for different catalysts can be arranged as follows (Fig. 7c and Table 2): 0.5%Tm-TiO_2 (93.1%) > 0.3%Tm-TiO_2 (90.7%) > 0.1%Tm-TiO_2 (81.2%) > TiO_2 (42.8%). The reaction rate (min^{-1}) of 0.5%Tm-TiO_2, 0.3%Tm-TiO_2, 0.1%Tm-TiO_2 and TiO_2 was 0.0325, 0.0245, 0.0234 and 0.0121, respectively (Fig. 7d). The improved photodegradation efficiency can be attributed to the increased adsorption capacity and the enhanced charge separation process. It was observed that the removal efficiency and degradation rate of *o*-xylene was slightly lower than that of acetaldehyde, which might due to the stronger affinity of acetaldehyde towards the catalyst surface than *o*-xylene. Also, the required energy for breaking the C = C (607 kJ/mol) bond of *o*-xylene is greater than the C–C (345.6 kJ/mol) bond of acetaldehyde. Meanwhile, the generation of free radicals (•OH and $•O_2^-$) was also responsible for enhancing the photocatalytic performance, a detail discussion is given in section 3.6.1.

3.5. Adsorption capacity and photocatalytic properties of mixed VOCs

Generally, several kinds of VOCs coexist in the atmosphere, thus, we carried out photocatalytic experiments on two typical coexisting VOCs. Based on our adsorption and degradation results, 0.5%Tm-TiO_2 sample was selected to perform adsorption and degradation experiments of mixed VOCs due to its excellent performance (Figs. 8, 9 and Fig. S6). The adsorption results of single acetaldehyde and *o*-xylene on pure and 0.5%Tm modified TiO_2 were used as a reference. Interestingly, the adsorption performance of single VOC was quite the opposite to the mixture (Fig. 8). Pure TiO_2 demonstrated lower adsorption capacity for

Table 2
The photocatalytic properties of the as-synthesized catalysts towards single VOC and mixed VOCs.

Condition	Properties	VOC type	Pure-TiO_2	0.1%Tm-TiO_2	0.3%Tm-TiO_2	0.5%Tm-TiO_2
Single VOC	Adsorption capacity (μmol/g)	acetaldehyde	1.083	1.845	2.545	3.635
		o-xylene	0.770	1.040	1.695	2.116
	Removal efficiency (%)	acetaldehyde	51.1	85.8	95.9	99.2
		o-xylene	42.8	81.2	90.7	93.1
Mixture VOCs (The ratio of acetaldehyde/o-xylene is 1:1)	Adsorption capacity (μmol/g)	acetaldehyde	0.615	–	–	1.885
		o-xylene	1.565	–	–	3.076
	Removal efficiency (%)	acetaldehyde	20.9	–	–	55.2
		o-xylene	31.8	–	–	99.7

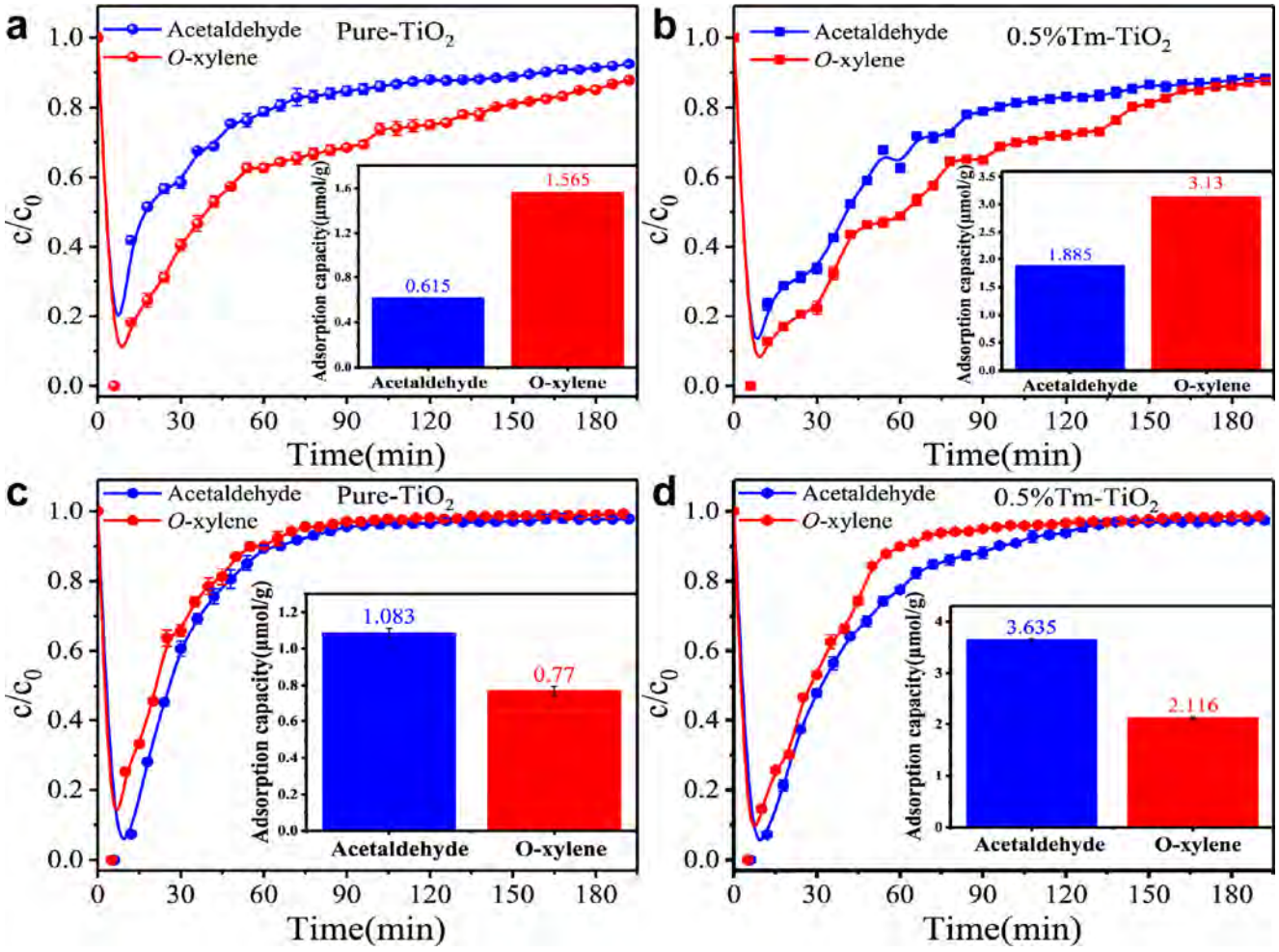

Fig. 8. Dynamic adsorption of the mixture of acetaldehyde and *o*-xylene on (a) pure TiO_2 and (b) 0.5%Tm-TiO_2 samples, and the adsorption of single VOC on (c) pure TiO_2 and (d) 0.5%Tm-TiO_2 catalysts. The insets show adsorption amount.

acetaldehyde (0.615 μmol/g) than that of *o*-xylene (1.565 μmol/g) in mixed VOCs (Fig. 8a and Table 2), but TiO_2 showed higher adsorption capacity for acetaldehyde (1.083 μmol/g) than *o*-xylene (0.770 μmol/g) with single pollutant (Fig. 8c and Table 2). Similarly, the adsorption amount of acetaldehyde (1.885 μmol/g for 0.5%Tm-TiO_2) was less than *o*-xylene (3.076 μmol/g for 0.5%Tm-TiO_2) under mixture mode (Fig. 8b Table 2), while the adsorption capacity of 0.5%Tm-TiO_2 sample for acetaldehyde (3.635 μmol/g) was more than *o*-xylene (2.116 μmol/g) under single mode (Fig. 8d and Table 2). One reason for this might be that when larger volume of *o*-xylene molecules adsorbed on the catalyst surface, it covers most of the adsorption sites, which might affect acetaldehyde adsorption. Another reason might be that the aldehyde group could be conjugated to aromatic rings after being adsorbed on the catalyst surface, thereby promoting the adsorption of *o*-xylene [49]. The adsorption capacity of 0.5%Tm-TiO_2 (1.885 μmol for acetaldehyde and 3.876 μmol for *o*-xylene, respectively) was larger than TiO_2 (0.615 μmol for acetaldehyde and 1.565 μmol for *o*-xylene, respectively) for the same VOC under mixture mode.

The differences in adsorption behavior have a significant effect on photocatalytic degradation properties, Fig. 9 provides a direct evidence for this behavior. The photocatalytic activity of the mixture was quite different from that of an individual contaminate. The removal efficiency of acetaldehyde (20.9% for TiO_2 and 55.2% for Tm-TiO_2 sample) was lower than *o*-xylene (31.8% for TiO_2 and 99.7% for Tm-TiO_2 sample) in the case of mixed VOCs (Fig. 9a, b and Table 2), while the photocatalytic efficiency of acetaldehyde (51.1% for TiO_2 and 99.2% for Tm-TiO_2 sample) was higher than *o*-xylene (42.8% for TiO_2 and 93.1% for Tm-TiO_2 sample) in single VOC mode (Fig. 9c, d and Table 2). This might be due to the fact that the opposite tendency of the adsorption capacity between the single VOC and mixed VOCs. Notably, 0.5%Tm-TiO_2 catalyst still maintained high photocatalytic performance under high adsorption capacity in mixed mode, in which the amount of acetaldehyde and *o*-xylene adsorbed by 0.5%Tm-TiO_2 was 3.1 and 2.0 times as much as pure sample, respectively. And no obvious deactivation was observed in 0.5%Tm-TiO_2 sample, even though the photocatalytic reaction time reached 300 min. Interestingly, the ratio of C to C_0 of pure sample decreased rapidly (Fig. 9a) while that of Tm modified sample first increased and then decreased in 50 min under light irradiation (Fig. 9b). It is due to the fact that 0.5%Tm-TiO_2 adsorbed larger quantity of mixed-VOCs than pure sample (Table 2). It is anticipated that the exposed reactive sites of 0.5%Tm-TiO_2 will decrease with increasing absorptivity, which will ultimately deteriorate the photodegradation efficiency. Accordingly, the desorption rate of VOC was higher than degradation and adsorption rate in 30 min, and consequently showing the negative removal efficiency value [50]. As the illumination time reached 48 min, most of the VOC molecules adsorbed by the catalyst have been desorbed. As a result, the covered reaction sites were gradually exposed, and then the degradation rate was larger than desorption and adsorption rates, thereby exhibiting the positive photocatalytic efficiency value (Fig. 9b). Also, pure TiO_2 began to inactivate after the illumination of 30 min, but 0.5%Tm-TiO_2 was poisoned after 300 min of operation. This phenomenon might be due to the fact that 0.5%Tm-TiO_2 had greater number of free radicals to photodegrade the intermediates in contrast to pristine TiO_2. Eventually, two

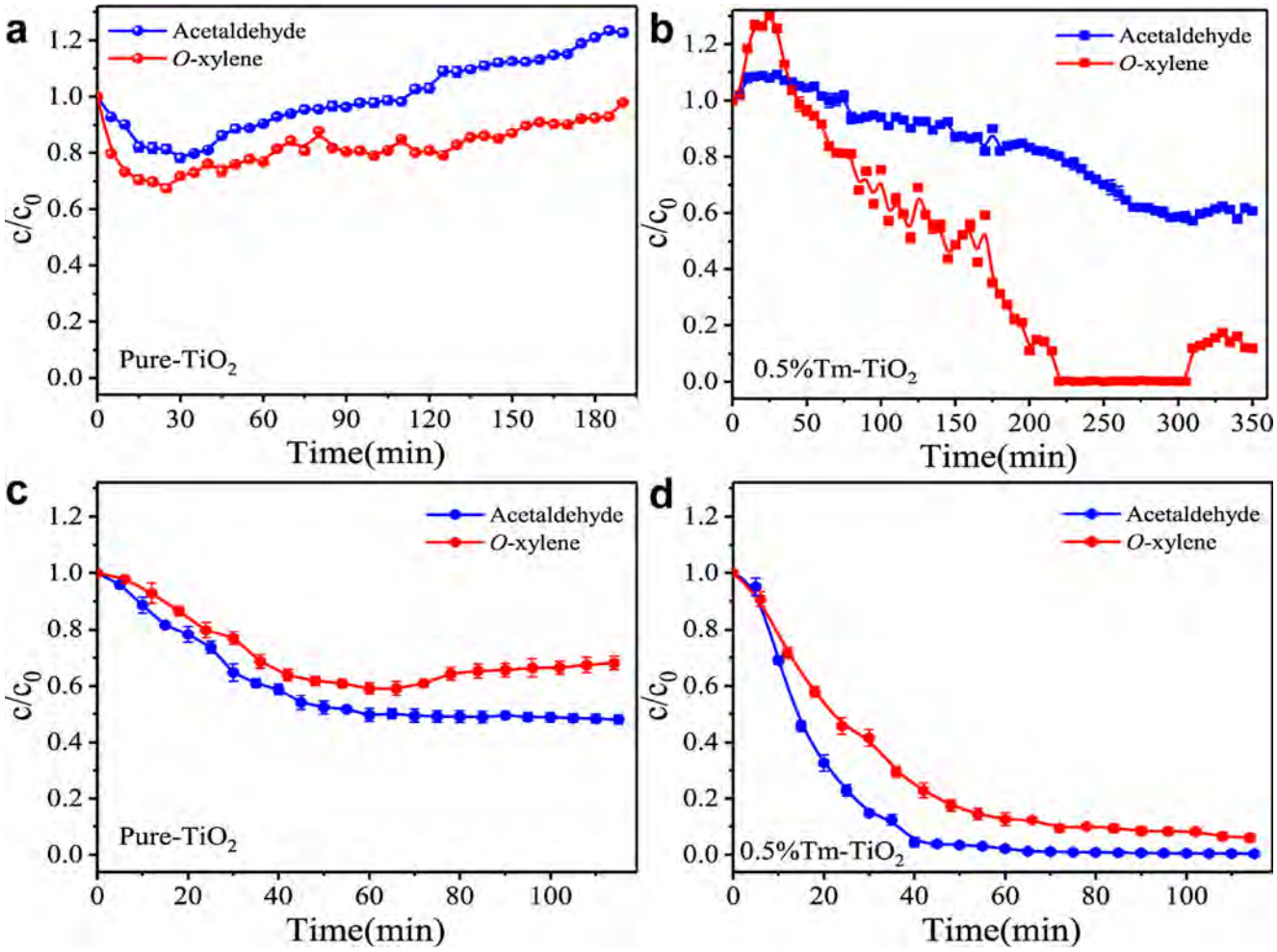

Fig. 9. Photodegradation plots of (a) pure TiO_2 and (b) 0.5%Tm-TiO_2 samples for mixed VOCs, and photodegradation curves of (c) pure TiO_2 and (d) 0.5%Tm-TiO_2 catalysts for single VOC.

catalysts were poisoned due to the formation of intermediates occupying the reactive sites on the catalyst surface. A detailed discussion of this has been presented in our previous work [24].

3.6. Proposed mechanism

3.6.1. Mechanism of photocatalytic activity enhancement

The Hydroxyl (•OH) and superoxide radicals ($\bullet O_2^-$) are important reactive species in the photocatalytic oxidation reaction [51]. We carried out ESR tests using DMPO as the spin-trapping agent to analyze the production of free radicals (•OH and $\bullet O_2^-$) for Tm-modified and unmodified TiO_2 samples. Fig. 10 shows the four-line ESR signal with a characteristic intensity ratio of 1:1:1 and 1:2:2:1, which were assigned to $\bullet O_2^-$ and •OH adducts, respectively [52,53]. This indicated that there existed $\bullet O_2^-$ and •OH active species involved in the removal of selected gaseous pollutants [51]. The intensities of $\bullet O_2^-$ (Fig. 10a) and •OH (Fig. 10b) increased with increasing Tm content in contrast to pure TiO_2, which suggested that the production of the reactive oxygen species was improved by Tm incorporation in TiO_2. This was attributed to the special intra-4f electronic structure of Tm accelerating photogenerated carries separation of the catalyst (Fig. 5). The PL and photoelectrochemical results further confirmed this behavior. Meanwhile, the enhancement in the hydrophilicity (OH groups) (Table 1 and Fig. S4) of the catalyst surface resulted in the formation of more •OH radicals. The greater number of reactive oxygen radicals will undoubtedly increase the photocatalytic activity, which was observed in our photocatalytic test.

Considering above, it can be inferred that an enhanced photoactive species production and adsorption capacity promoted the photocatalytic activity of the catalyst. A proposed mechanism for enhancing the photocatalytic performance of TiO_2-based catalysts is presented in Scheme 1. TiO_2 modified with Tm ions (introducing the new Tm-4f level) promoted the separation efficiency of photoinduced electron-hole pairs, thereby generating more photoactive species to increase photocatalytic properties for removing the target VOCs.

3.6.2. Photocatalytic degradation pathway under single VOC

GC–MS was carried out to disclose the photocatalytic degradation pathway of pure TiO_2 and 0.5%Tm-TiO_2 sample for *o*-xylene and mixture (acetaldehyde and *o*-xylene). As indicated in Fig. 11, the intermediates of pure TiO_2 in the case of *o*-xylene (Fig. 11a) showed chemical compound specified as 2, 6, 7, 9, 10, 11 and 12 while that of 0.5%Tm-TiO_2 (Fig. 11b) did not produce intermediates 7 and 10. The presence of *o*-xylene (No.1) showed some undegraded residues, which was observed in all samples.

Based on the GC- MS signals, the proposed photocatalytic reaction route in single VOC mode is shown in Scheme 2, Table 3, and Fig. S7. In the case of pure TiO_2, *o*-xylene (No. 1) was converted to *o*-benzaldehyde (No. 2), toluene (No. 6) and benzene (No. 7) [35–37], which were further oxidized into open chain compounds including butanol (No. 9), butanone (No. 10) and acetone (No. 11), and eventually mineralized into CO_2 (No. 12) and H_2O. However, no toluene and acetone were detected in the photodegradation process of *o*-xylene when 0.5%Tm-TiO_2 was used as the photocatalyst. This might be due to the presence of

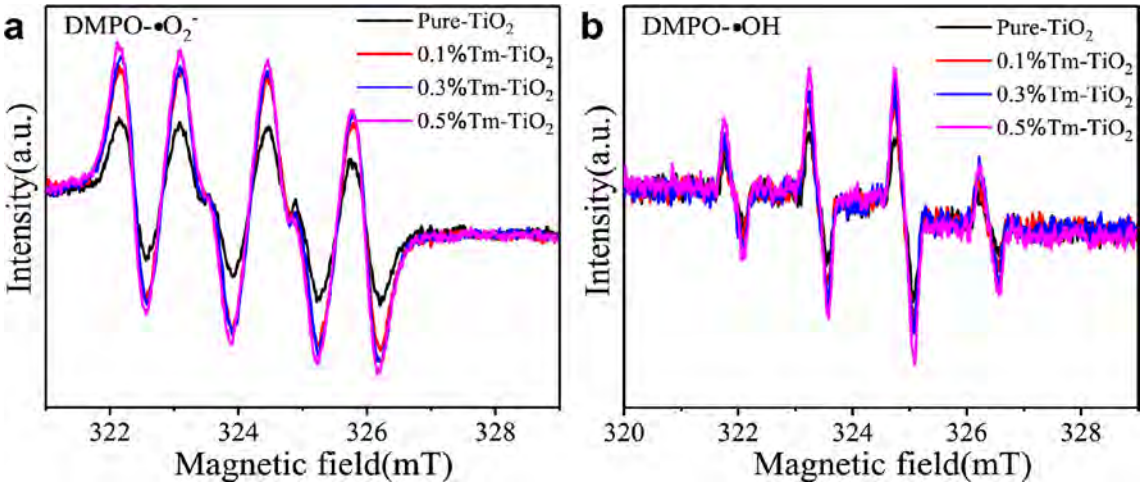

Fig. 10. ESR signals of DMPO- $\bullet O_2^-$ in ethanol dispersion (a) and DMPO- •OH in aqueous dispersion (b) of the as-prepared photocatalysts under 400 W xenon lamp irradiation for 4 min.

more reactive oxidation species in Tm-doped samples (shown in Fig. 10) which readily oxidize toluene into open ring products without generating benzene and mineralized acetone into CO_2 and H_2O or other products in contrast to pristine TiO_2. This is why the removal efficiency of Tm-TiO_2 was higher than pure TiO_2.

The proposed photodegradation routes of *o*-xylene on different photocatalysts in our work are quite different from previous studies. Liu et al. [54] suggested that thermal catalysis of *o*-xylene follow intermediates, such as 1,3-isobenzofurandione, citric acid and acetic acid utilizing γ-MnO_2/SMO at 220 ℃. Pei et al. [55] reported that various intermediate products (i.e., propanedioic acid, formic acid, acetic acid and oxalic acid) in the photodecomposition of *o*-xylene using a TiO_2/ZnO/Bi_2O_3 photocatalyst. We also detected benzene and toluene in our work despite variation in experimental conditions. However, the open chain intermediate species in our work are somewhat different. Wang et al. [56] investigated that TaON/V_2O_5 photocatalyst photodegraded *o*-xylene into benzyl alcohol, hydroxytoluene, methoxy acetaldehyde and xylose under visible light illumination. Overall, the photocatalytic degradation pathway and intermediates of *o*-xylene are closely related to the catalyst system and light source. Based on the previous work [54–59], even though toluene and *o*-xylene are aromatic compounds with similar properties, there still exist significant differences in their degradation pathways, especially in ring-opening products. Therefore, there are still too many problems to be solved in the photocatalytic degradation path of VOC, such as the relationship between intermediates and oxidation reactive species, the reasons for the formation

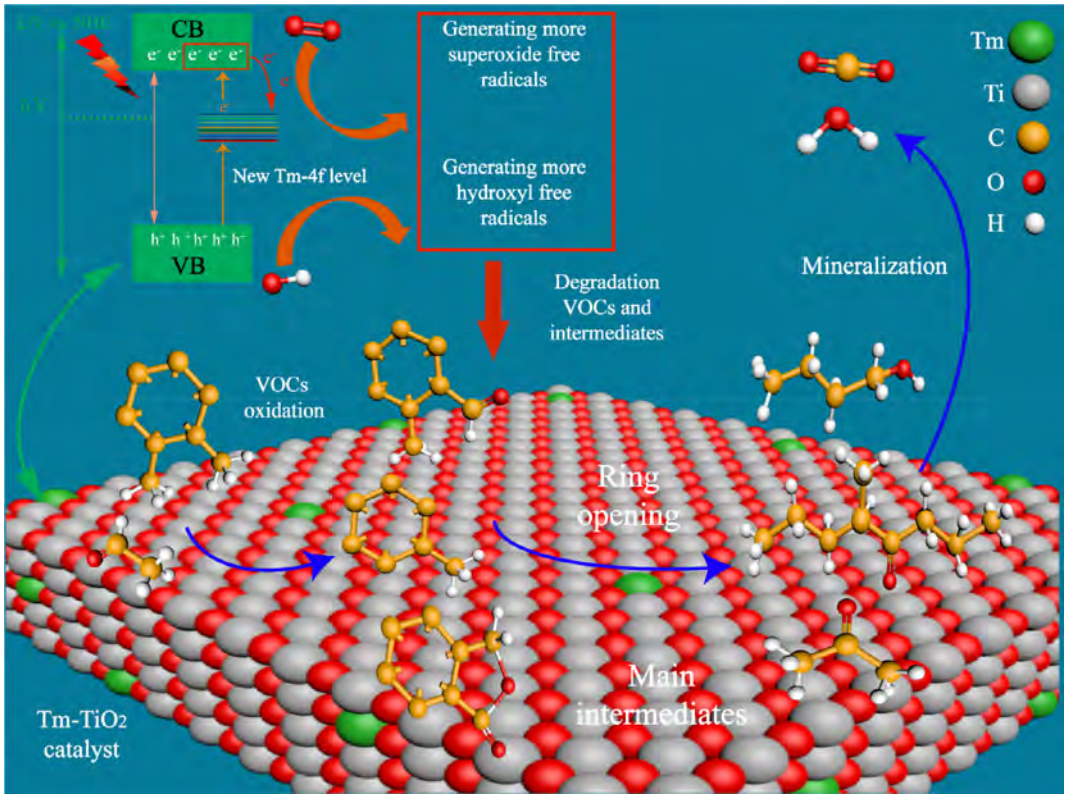

Scheme 1. Schematic diagram, which shows the mechanism of improving photocatalytic activity by Tm-induced 4f levels promoting electron-to-electron transfer transition between Tm and TiO_2.

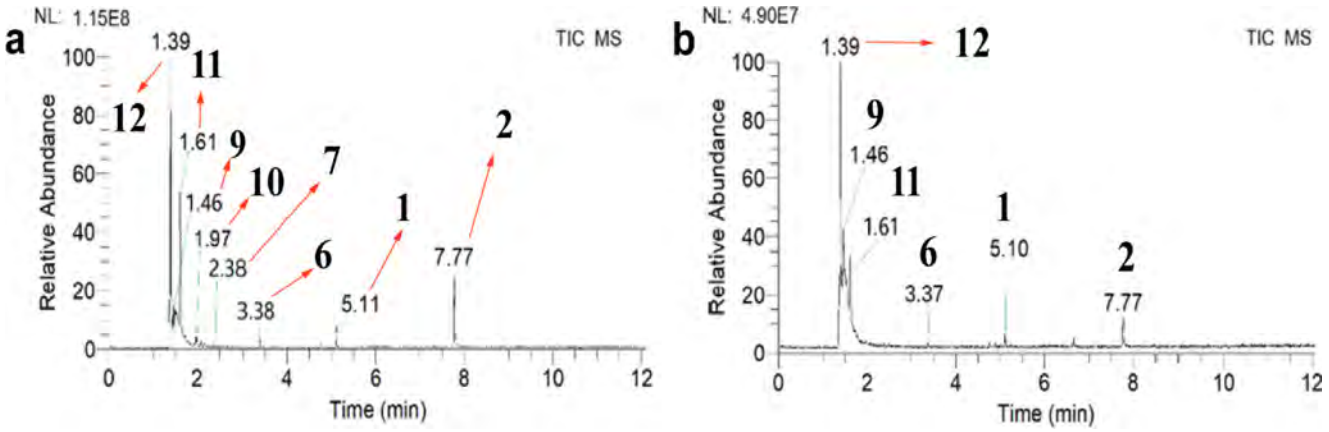

Fig. 11. MS signals of (a) pure TiO_2 and (b) 0.5%Tm-TiO_2 samples for single VOC.

of different intermediates, open-ring route of *o*-xylene and the role of photoactive species in degradation process.

3.6.3. Photocatalytic degradation pathway under mixed VOCs

Fig. 12 displays the formation of intermediates regarding acetaldehyde and *o*-xylene mixture photodegradation on pure and 0.5%Tm-doped TiO_2. Different chemical compounds were detected when pure TiO_2 was utilized as the photocatalysts in the reaction chamber, which are specified by numbers like 2, 3, 4, 5, 6, 8, 9, 10, 11 and 12 (Fig. 12a). In the case of 0.5%Tm-TiO_2, new by-product 7 was generated, however, compounds 3, 4 and 5 (Fig. 12b) could not be detected. Based on these results, we proposed possible oxidation reaction paths for acetaldehyde and *o*-xylene mixture on pure and Tm-doped TiO_2 (Scheme 3). It can be anticipated regarding pure TiO_2, that initially *o*-xylene was oxidized to toluene, phthalide, naphthalene and *o*-methyl acetophenone. Next, the aromatic ring containing compounds are converted to open chain products, i.e., 5-Methyl-4-octanone, butanol, butanone and acetone, and ultimately degraded to CO_2 and H_2O. Particularly, *o*-methyl acetophenone was produced through the reaction among intermediates of acetaldehyde and *o*-xylene. Instead of generating phthalide, naphthalene and *o*-methyl acetophenone, benzene was produced in 0.5%Tm-TiO_2. Obviously, the intermediates of Tm modified catalyst were less than that of pure sample, which might be due to the fact that the free radical yield rate of Tm doping sample was higher than that of pure sample. The intermediates of single and mixed VOCs were quite different. This might be attributed to the change of the adsorption behavior (Fig. 8a and c), the effect of introducing another VOC (the change of reaction environment system) and also the interaction among intermediates.

Therefore, it can be inferred that the yield of reactive oxidation species is the main factor, which affects the degradation pathway. Also, the difference in adsorption behavior (such as a change in the adsorption trends under mixed condition) might be a factor which can influence the reaction pathway for the same catalyst. Hence, we can achieve our desired oxidation reaction pathway by controlling the yield of reactive oxidation species and adsorption behavior of photocatalysts for the target VOCs.

4. Conclusion

In summary, photocatalytic oxidation of acetaldehyde, *o*-xylene, and their mixture on pure and Tm-modified TiO_2 was investigated. Tm doping induced new Tm-4f states in TiO_2, which facilitated charge transfer and hole-electron pairs separation as evidenced by

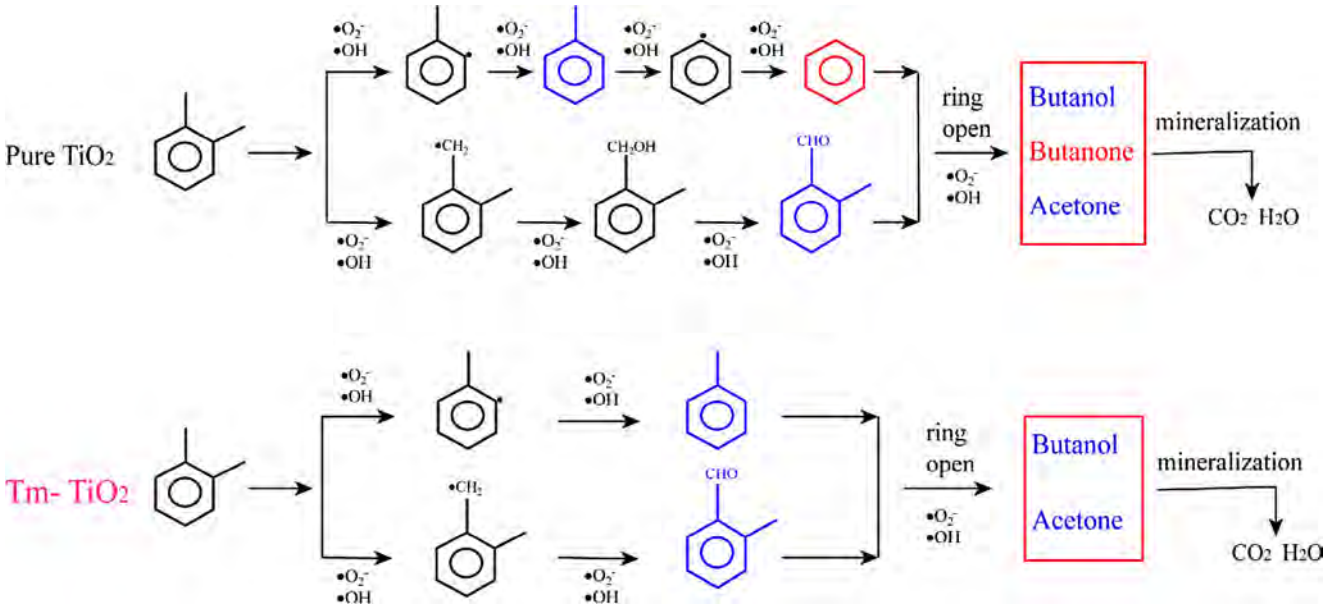

Scheme 2. The proposed photocatalytic degradation pathway of single VOC over the investigated catalysts, the red and blue products represent the photodegradation intermediates.

Table 3
Intermediate products of photocatalytic degradation of single *o*-xylene and mixed VOCs under the given experimental conditions.

Product No.	Name	Main fragment (*m/z*)	Retention time (min)	Formula	Structure
1	*o*-xylene	91, 106, 77	5.10	C_8H_{10}	
2	*o*-tolualdehyde	91, 119, 65	7.77	C_8H_8O	
3	Phthalide	105, 77, 134	11.06	$C_8H_6O_2$	
4	*o*-methylacetophenone	91,119, 65, 134	8.69	$C_9H_{10}O$	
5	Naphthalene	128, 127, 192	9.30	$C_{10}H_8$	
6	Toluene	91, 92, 65	3.38	C_7H_8	
7	Benzene	78, 86, 134	2.38	C_6H_6	
8	5-Methyl-4-octanone	43, 71, 114	3.70	$C_9H_{18}O$	
9	Butanol	44, 56, 57	1.46	$C_4H_{10}O$	
10	Butanone	43, 44, 72	1.97	C_4H_8O	
11	Acetone	43, 58, 59	1.61	C_3H_6O	
12	Carbon dioxide	44, 45	1.39	CO_2	

photocurrent, EIS and PL results, respectively. The presence of Tm_2O_3 on grain boundaries rendered a hydrophilic character, which facilitated the increase of adsorption capacity and the production of •OH radicals. The above two factors mainly contribute to the greatly enhanced photocatalytic performance of Tm-modified TiO_2. The adsorption and degradation of VOCs showed that the adsorption of acetaldehyde was higher than that of *o*-xylene for individual mode, while acetaldehyde showed decreased adsorption in mixture compared with *o*-xylene. In

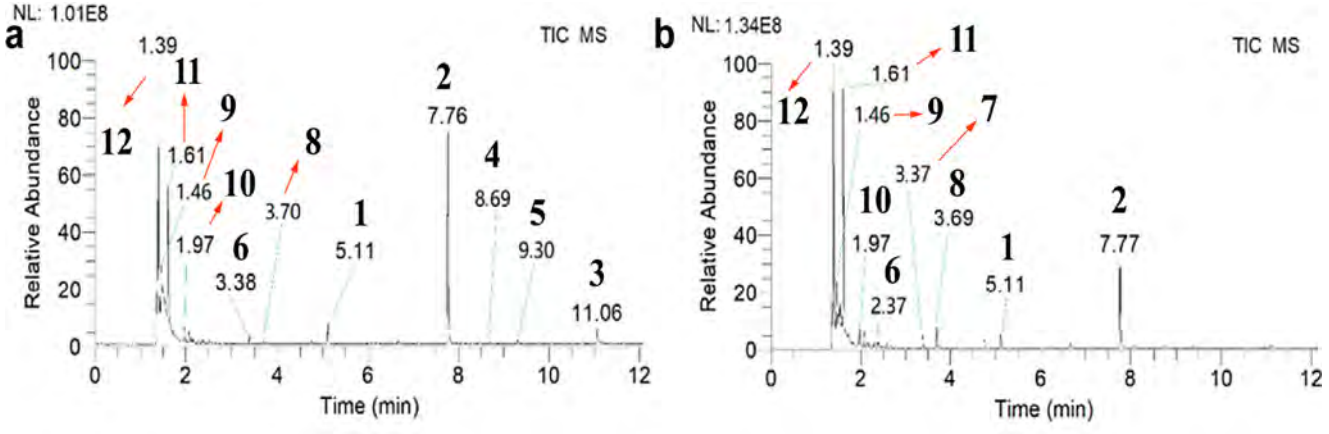

Fig. 12. MS signals of (a) pure TiO_2 and (b) 0.5%Tm-TiO_2 samples for mixed VOCs.

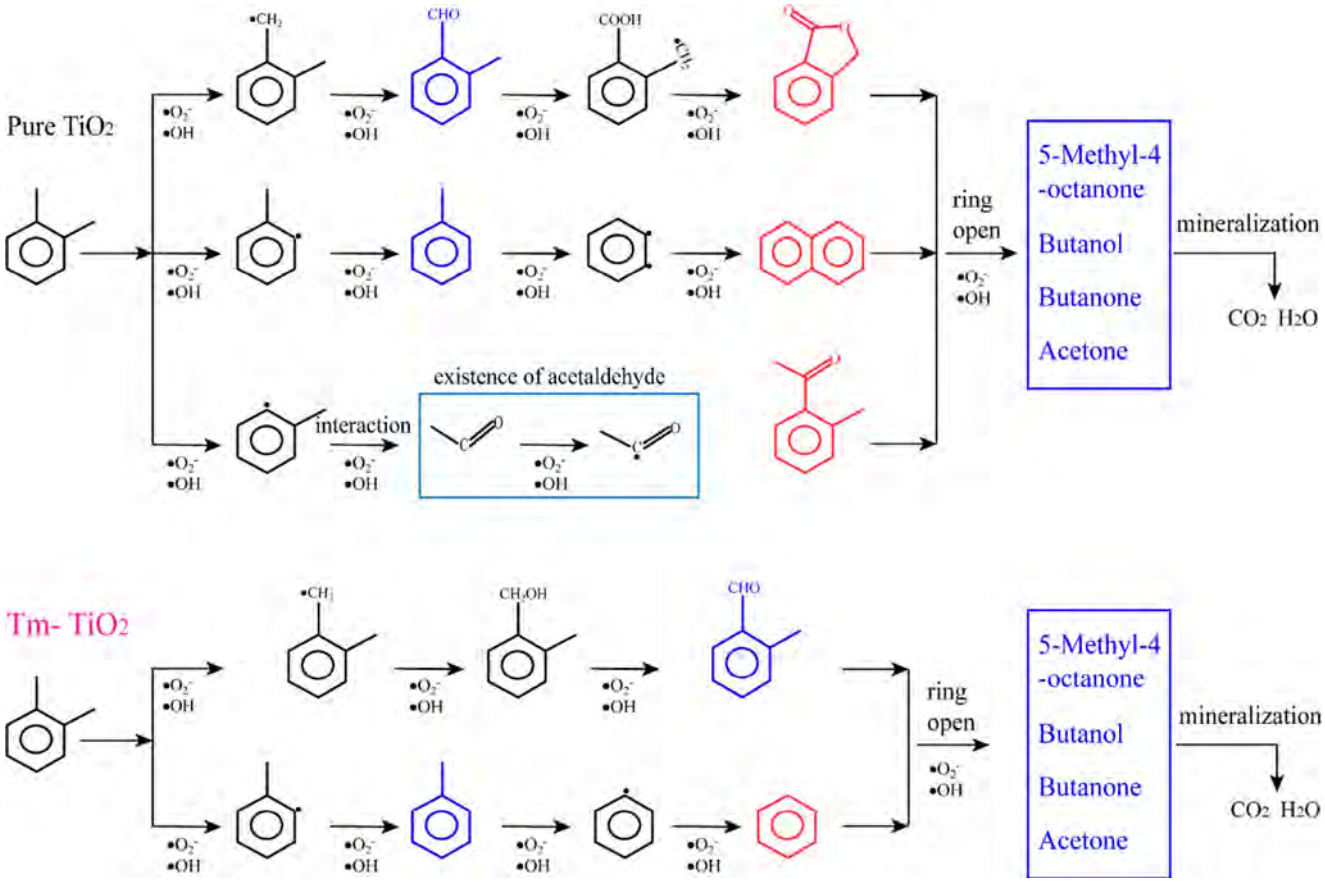

Scheme 3. The proposed photocatalytic degradation pathway of mixed VOCs over the investigated catalysts, the red and blue products represent the photo-degradation intermediates.

the single and mixed pollutants modes, the difference in the generation of the reactive species and adsorption behaviors led to the different degradation pathways. Our work provides an effective strategy to modify TiO_2 based catalyst for target VOCs degradation. It also has an important guiding significance for how to design a photocatalyst for the efficient degradation of mixed VOCs in the future.

Declaration of Competing Interest

The authors declare that they have no known competing financial interests or personal relationships that could have appeared to influence the work reported in this paper.

Acknowledgment

This work was financially supported by the National Key Research and Development Program of China (2016YFA0203000), the NSFC-DFG bilateral organization program (51761135107), the Youth Innovation Promotion Association CAS (2017042) and Shanghai Sailing Program (18YF1426800).

Appendix A. Supplementary data

Experimental setup for photocatalytic degradation VOC, TEM, HRTEM images and up-conversion spectra of 0.5%Tm-TiO_2 sample, XPS spectra for Ti 2p and C 1s regions and contact angles and EIS plots of catalysts, Blank dynamic adsorption curves under mixed VOCs, MS signals of the main fragment of the intermediate products No. 1- 12, Cyclic photocatalytic performances of 0.5%Tm-TiO_2 in the degradation of gaseous acetaldehyde, The XPS spectra of the 0.5%Tm-TiO_2 sample for (a) Ti 2p and (b) Tm 4d regions, CO_2 generation of acetaldehyde (a) and *o*-xylene (b) over pure and 0.5%Tm-TiO_2 photocatalysts.

Supplementary data to this article can be found online at https://doi.org/10.1016/j.cej.2020.125078.

References

[1] I. Riipinen, T. Yli-Juuti, J.R. Pierce, T. Petaja, D.R. Worsnop, M. Kulmala, N.M. Donahue, The contribution of organics to atmospheric nanoparticle growth, Nat. Geosci. 5 (2012) 453–458.
[2] N.L. Ng, J.H. Kroll, A.W.H. Chan, P.S. Chhabra, R.C. Flagan, J.H. Seinfeld, Secondary organic aerosol formation from m-xylene, toluene, and benzene, Atmos. Chem. Phys. 7 (2007) 3909–3922.
[3] R.-J. Huang, Y. Zhang, C. Bozzetti, K.-F. Ho, J.-J. Cao, Y. Han, K.R. Daellenbach, J.G. Slowik, S.M. Platt, F. Canonaco, P. Zotter, R. Wolf, S.M. Pieber, E.A. Bruns, M. Crippa, G. Ciarelli, A. Piazzalunga, M. Schwikowski, G. Abbaszade, J. Schnelle-Kreis, R. Zimmermann, Z. An, S. Szidat, U. Baltensperger, I. El Haddad, A.S.H. Prevot, High secondary aerosol contribution to particulate pollution during haze events in China, Nature 514 (2014) 218–222.
[4] M.R. Hoffmann, S.T. Martin, W.Y. Choi, D.W. Bahnemann, Environmental applications of semiconductor photocatalysis, Chem. Rev. 95 (1995) 69–96.
[5] R.M. Alberici, W.F. Jardim, Photocatalytic destruction of VOCs in the gas-phase using titanium dioxide, Appl. Catal. B: Environ. 14 (1997) 55–68.
[6] S.W. Verbruggen, TiO_2 photocatalysis for the degradation of pollutants in gas phase: from morphological design to plasmonic enhancement, J. Photoch. Photobio. C. 24 (2015) 64–82.
[7] Z. Shayegan, C.-S. Lee, F. Haghighat, TiO_2 photocatalyst for removal of volatile organic compounds in gas phase –A review, Chem. Eng. J. 334 (2018) 2408–2439.
[8] D.-H. Wang, L. Jia, X.-L. Wu, L.-Q. Lu, A.-W. Xu, One-step hydrothermal synthesis of N-doped TiO_2/C nanocomposites with high visible light photocatalytic activity, Nanoscale 4 (2012) 576–584.
[9] X. Zhou, N. Liu, P. Schmuki, Photocatalysis with TiO_2 nanotubes: “colorful” reactivity and designing site-specific photocatalytic centers into TiO_2 nanotubes, ACS Catal. 7 (2017) 3210–3235.
[10] T. Sun, Y. Chen, X.-Q. Ma, Z. Li, H. Li, X.-L. Cui, Facile synthesis of visible light activated carbon-incorporated Mn doped TiO_2 microspheres via flame thermal method, J. Inorg. Mater. 30 (2015) 1002–1008.
[11] W. Zheng, P. Huang, D. Tu, E. Ma, H. Zhu, X. Chen, Lanthanide-doped upconversion

nano-bioprobes: electronic structures, optical properties, and biodetection, Chem. Soc. Rev. 44 (2015) 1379–1415.
[12] J. Zhou, Q. Liu, W. Feng, Y. Sun, F. Li, Upconversion luminescent materials: advances and applications, Chem. Rev. 115 (2015) 395–465.
[13] M.-K. Tsang, G. Bai, J. Hao, Stimuli responsive upconversion luminescence nanomaterials and films for various applications, Chem. Soc. Rev. 44 (2015) 1585–1607.
[14] P. Parnicka, P. Mazierski, T. Grzyb, Z. Wei, E. Kowalska, B. Ohtani, W. Lisowski, T. Klimczuk, J. Nadolna, Preparation and photocatalytic activity of Nd-modified TiO_2 photocatalysts: Insight into the excitation mechanism under visible light, J. Catal. 353 (2017) 211–222.
[15] P. Mazierski, A. Mikolajczyk, B. Bajorowicz, A. Malankowska, A. Zaleska-Medynska, J. Nadolna, The role of lanthanides in TiO_2-based photocatalysis: a review, Appl. Catal. B: Environ. 233 (2018) 301–317.
[16] J. Reszczynska, T. Grzyb, J.W. Sobczak, W. Lisowski, M. Gazda, B. Ohtani, A. Zaleska, Visible light activity of rare earth metal doped (Er^{3+}, Yb^{3+} or Er^{3+}/Yb^{3+}) titania photocatalysts, Appl. Catal. B: Environ. 163 (2015) 40–49.
[17] S. Obregon, A. Kubacka, M. Fernandez-Garcia, G. Colon, High-performance Er^{3+}-TiO_2 system: Dual up-conversion and electronic role of the lanthanide, J. Catal. 299 (2013) 298–306.
[18] P. Mazierski, P.N.A. Caicedo, T. Grzyb, A. Mikolajczyk, J.K. Roy, E. Wyrzykowska, Z. Wei, E. Kowalska, T. Puzyn, A. Zaleska-Medynska, J. Nadolna, Experimental and computational study of Tm-doped TiO_2: The effect of Li^+ on Vis-response photocatalysis and luminescence, Appl. Catal. B: Environ. 252 (2019) 138–151.
[19] D.M. De los Santos, J. Navas, T. Aguilar, A. Sanchez-Coronilla, C. Fernandez-Lorenzo, R. Alcantara, J. Carlos Pinero, G. Blanco, J. Martin-Calleja, Tm-doped TiO_2 and $Tm_2Ti_2O_7$ pyrochlore nanoparticles: enhancing the photocatalytic activity of rutile with a pyrochlore phase, Beilstein J. Nanotechnol. 6 (2015) 605–616.
[20] J. Navas, A. Sanchez-Coronilla, T. Aguilar, D.M. De los Santos, N.C. Hernandez, R. Alcantara, C. Fernandez-Lorenzo, J. Martin-Calleja, Thermo-selective TmxTi1-xO_2-x/2 nanoparticles: from Tm-doped anatase TiO_2 to a rutile/pyrochlore $Tm_2Ti_2O_7$ mixture. An experimental and theoretical study with a photocatalytic application, Nanoscale 6 (2014) 12740–12757.
[21] D.M. de los Santos, J. Navas, T. Aguilar, A. Sanchez-Coronilla, R. Alcantara, C. Fernandez-Lorenzo, G. Blanco, J. Martin Calleja, Study of thulium doping effect and enhancement of photocatalytic activity of rutile TiO_2 nanoparticles, Mater. Chem. Phys. 161 (2015) 175–184.
[22] A.W. Xu, Y. Gao, H.Q. Liu, The preparation, characterization, and their photocatalytic activities of rare-earth-doped TiO_2 nanoparticles, J. Catal. 207 (2002) 151–157.
[23] J. Sivasankari, S. Sankar, S. Selvakumar, L. Vimaladevi, R. Krithiga, Synthesis, structural and optical properties of Er doped, Li doped and Er plus Li co-doped ZnO nanocrystallites by solution-combustion method, Mater. Chem. Phys. 143 (2014) 1528–1535.
[24] Z. Rao, X. Xie, X. Wang, A. Mahmood, S. Tong, M. Ge, J. Sun, Defect chemistry of Er^{3+}-doped TiO_2 and its photocatalytic activity for the degradation of flowing gas-phase VOCs, J. Phys. Chem. C 123 (2019) 12321–12334.
[25] S.J. Armaković, M. Grujić-Brojčin, M. Šćepanović, S. Armaković, A. Golubović, B. Babić, B.F. Abramović, Efficiency of La-doped TiO_2 calcined at different temperatures in photocatalytic degradation of β-blockers, Arab. J. Chem. (2017).
[26] W. Li, A.I. Frenkel, J.C. Woicik, C. Ni, S.I. Shah, Dopant location identification in Nd^{3+}-doped TiO_2 nanoparticles, Phys. Rev. B 72 (2005) 155315.
[27] M. Meksi, A. Turki, H. Kochkar, L. Bousselmi, C. Guillard, G. Berhault, The role of lanthanum in the enhancement of photocatalytic properties of TiO_2 nanomaterials obtained by calcination of hydrogenotitanate nanotubes, Appl. Catal. B: Environ. 181 (2016) 651–660.
[28] T. Ohsaka, F. Izumi, Y. Fujiki, Raman-spectrum of anatase, TiO_2, J. Raman Spectrosc. 7 (1978) 321–324.
[29] E. Haroponiatowski, R. Rodrigueztalavera, M. Delacruzheredia, O. Canocorona, R. Arroyomurillo, Crystallization of nanosized titania particles prepared by the sol-gel process, J. Mater. Res. 9 (1994) 2102–2108.
[30] F. Tian, Y. Zhang, J. Zhang, C. Pan, Raman spectroscopy: A new approach to measure the percentage of anatase TiO_2 exposed (001) facets, J. Phys. Chem. C 116 (2012) 7515–7519.
[31] P. Peterka, I. Kasik, A. Dhar, B. Dussardier, W. Blanc, Theoretical modeling of fiber laser at 810 nm based on thulium-doped silica fibers with enhanced H-3(4) level lifetime, Opt. Express 19 (2011) 2773–2781.
[32] B. Zhou, H. Lin, E.Y.-B. Pun, Tm^{3+}-doped tellurite glasses for fiber amplifiers in broadband optical communication at 1.20 mu m wavelength region, Opt. Express 18 (2010) 18805–18810.
[33] J. Castaneda-Contreras, V.F. Maranon-Ruiz, R. Chiu-Zarate, H. Perez-Ladron de Guevara, R. Rodriguez, C. Michel-Uribe, Photocatalytic activity of erbium-doped TiO_2 nanoparticles immobilized in macro-porous silica films, Mater. Res. Bull. 47 (2012) 290–295.
[34] P. Mazierski, W. Lisowski, T. Grzyb, M.J. Winiarski, T. Klimczuk, A. Mikolajczyk, J. Flisikowski, A. Hirsch, A. Kolakowska, T. Puzyn, A. Zaleska-Medynska, J. Nadolna, Enhanced photocatalytic properties of lanthanide-TiO_2 nanotubes: An experimental and theoretical study, Appl. Catal. B: Environ. 205 (2017) 376–385.
[35] Y. Liu, S. Zhou, J. Li, Y. Wang, G. Jiang, Z. Zhao, B. Liu, X. Gong, A. Duan, J. Liu, Y. Wei, L. Zhang, Photocatalytic reduction of CO_2 with water vapor on surface La-modified TiO_2 nanoparticles with enhanced CH_4 selectivity, Appl. Catal. B: Environ. 168 (2015) 125–131.
[36] J.-Y. Eom, S.-J. Lim, S.-M. Lee, W.-H. Ryu, H.-S. Kwon, Black titanium oxide nanoarray electrodes for high rate Li-ion microbatteries, J. Mater. Chem. A 3 (2015) 11183–11188.
[37] J.G. Yu, X.J. Zhao, Q.N. Zhao, Effect of film thickness on the grain size and photocatalytic activity of the sol-gel derived nanometer TiO_2 thin films, J. Mater. Sci. Lett. 19 (2000) 1015–1017.
[38] A. Rjeb, S. Letarte, L. Tajounte, M.C. El Idrissi, A. Adnot, D. Roy, Y. Claire, J. Kaloustian, Polypropylene natural aging studied by X-ray photoelectron spectroscopy, J. Electron Spectrosc. Relat. Phenom. 107 (2000) 221–230.
[39] P. Mazierski, M. Nischk, M. Golkowska, W. Lisowski, M. Gazda, M.J. Winiarski, T. Klimczuk, A. Zaleska-Medynska, Photocatalytic activity of nitrogen doped TiO_2 nanotubes prepared by anodic oxidation: The effect of applied voltage, anodization time and amount of nitrogen dopant, Appl. Catal. B: Environ. 196 (2016) 77–88.
[40] Y. Wang, J. Cai, M. Wu, H. Zhang, M. Meng, Y. Tian, T. Ding, J. Gong, Z. Jiang, X. Li, Hydrogenated cagelike titania hollow spherical photocatalysts for hydrogen evolution under simulated solar light irradiation, ACS Appl. Mater. & Inter. 8 (2016) 23006–23014.
[41] X. Chen, L. Liu, P.Y. Yu, S.S. Mao, Increasing solar absorption for photocatalysis with black hydrogenated titanium dioxide nanocrystals, Science 331 (2011) 746–750.
[42] Y. Uwamino, T. Ishizuka, H. Yamatera, X-ray photoelectron-spectroscopy of rare-earth compounds, J. Electron Spectrosc. Relat. Phenom. 34 (1984) 67–78.
[43] R. Imani, R. Dillert, D.W. Bahnemann, M. Pazoki, T. Apih, V. Kononenko, N. Repar, V. Kralj-Iglic, G. Boschloo, D. Drobne, T. Edvinsson, A. Iglic, Multifunctional gadolinium-doped mesoporous TiO_2 nanobeads: photoluminescence, enhanced spin relaxation, and reactive oxygen species photogeneration, beneficial for cancer diagnosis and treatment, Small 13 (2017).
[44] X. Chen, W. Luo, Optical spectroscopy of rare earth ion-doped TiO_2 nanophosphors, J. Nanosci. Nanotechno. 10 (2010) 1482–1494.
[45] X. Zhou, V. Haeublein, N. Liu, N. Nhat Truong, E.M. Zolnhofer, H. Tsuchiya, M.S. Killian, K. Meyer, L. Frey, P. Schmuki, TiO_2 nanotubes: nitrogen-ion implantation at low dose provides noble-metal-free photocatalytic H_2-evolution activity, Angew. Chem. Int. Edit. 55 (2016) 3763–3767.
[46] Z. Xu, J. Yu, Visible-light-induced photoelectrochemical behaviors of Fe-modified TiO_2 nanotube arrays, Nanoscale 3 (2011) 3138–3144.
[47] J.S. Lee, K.H. You, C.B. Park, Highly photoactive, low bandgap TiO_2 nanoparticles wrapped by graphene, Adv. mater. 24 (2012) 1084–1088.
[48] C.L. Bianchi, S. Gatto, C. Pirola, A. Naldoni, A. Di Michele, G. Cerrato, V. Crocella, V. Capucci, Photocatalytic degradation of acetone, acetaldehyde and toluene in gas-phase: Comparison between nano and micro-sized TiO_2, Appl. Catal. B: Environ. 146 (2014) 123–130.
[49] A.H. Mamaghani, F. Haghighat, C.-S. Lee, Photocatalytic oxidation technology for indoor environment air purification: The state-of-the-art, Appl. Catal. B: Environ. 203 (2017) 247–269.
[50] Y. Hu, X. Xie, X. Wang, Y. Wang, Y. Zeng, D.Y.H. Pui, J. Sun, Visible-light upconversion carbon quantum dots decorated TiO_2 for the photodegradation of flowing gaseous acetaldehyde, Appl. Sur. Sci. 440 (2018) 266–274.
[51] Y. Nosaka, A.Y. Nosaka, Generation and detection of reactive oxygen species in photocatalysis, Chem. Rev. 117 (2017) 11302–11336.
[52] H. Zhang, H. Huang, H. Ming, H. Li, L. Zhang, Y. Liu, Z. Kang, Carbon quantum dots/Ag_3PO_4 complex photocatalysts with enhanced photocatalytic activity and stability under visible light, J. Mater. Chem. 22 (2012) 10501–10506.
[53] W. Zhang, Y. Sun, F. Dong, W. Zhang, S. Duan, Q. Zhang, Facile synthesis of organic inorganic layered nanojunctions of g-C_3N_4/$(BiO)_2CO_3$ as efficient visible light photocatalystt, Dalton T. 43 (2014) 12026–12036.
[54] L. Liu, J. Li, H. Zhang, L. Li, P. Zhou, X. Meng, M. Guo, J. Jia, T. Sun, In situ fabrication of highly active gamma-MnO_2/$SmMnO_3$ catalyst for deep catalytic oxidation of gaseous benzene, ethylbenzene, toluene, and o-xylene, J. Hazard. Mater. 362 (2019) 178–186.
[55] C.C. Pei, W.W.-F. Leung, Photocatalytic oxidation of nitrogen monoxide and o-xylene by TiO_2/ZnO/Bi_2O_3 nanofibers: Optimization, kinetic modeling and mechanisms, Appl. Catal. B: Environ. 174 (2015) 515–525.
[56] S. Wang, Z. Li, Y. Guan, L. Lu, Z. Shi, P. Weng, S. Yan, Z. Zou, Visible light driven TaON/V_2O_5 heterojunction photocatalyst for deep elimination of volatile-aromatic compounds, Appl. Catal. B: Environ. 245 (2019) 220–226.
[57] P. Zhang, J. Huang, J. Shu, B. Yang, Comparison of secondary organic aerosol (SOA) formation during o-, m-, and p-xylene photooxidation, Environ. Pollut. 245 (2019) 20–28.
[58] M. Sleiman, P. Conchon, C. Ferronato, J.-M. Chovelon, Photocatalytic oxidation of toluene at indoor air levels (ppbv): Towards a better assessment of conversion, reaction intermediates and mineralization, Appl. Catal. B: Environ. 86 (2009) 159–165.
[59] H. Wu, L. Wang, Z. Shen, J. Zhao, Catalytic oxidation of toluene and p-xylene using gold supported on Co_3O_4 catalyst prepared by colloidal precipitation method, J. Mol. Catal. A: Chem. 351 (2011) 188–195.